

Rigor, and plan-view simulation of surfaces

L.D. Marks

Center for Surface Radiation Damage Studies, Department of Materials Science and Engineering, Northwestern University, Evanston, IL 60208, USA

Received 11 June 1991

This paper discusses the rigor of simulating plan-view images of surfaces using numerical multislice calculations. In particular, the validity of using a conventional multislice approach with individual atomic slices is tested versus a three-dimensional multislice with the top and bottom surfaces specifically included; the result is that the two are identical when inelastic scattering is neglected and almost identical when it is included. These results also demonstrate that inelastic scattering cannot be neglected for surface plan-view simulations. For instance, the bulk-forbidden, surface-allowed spots are shown to correspond to true bulk Bloch waves which are damped in thicker crystals consistent with experimental observations. The existence of a strong top–bottom effect is also pointed out, which means that plan-view imaging is more sensitive to the bottom surface except in exceedingly thin crystals.

1. Introduction

The technical and scientific importance of surfaces is well known, but despite many years of study there are still many unknowns. One of the reasons for this is that the most basic feature, namely the surface structure, has proved difficult in many cases to unambiguously determine experimentally. Until very recently essentially all the techniques available utilized diffraction (scattering), and were only able to probe the average component of the surface. There were major problems for the inhomogeneous elements of the surface because of the phase problem; information about the position of features is typically contained in the phase of scattered waves which is lost in a reciprocal space experiment. STM has clearly produced a revolution in the quality and quantity of information available concerning surface structures, but it does have one fundamental limitation: it is only sensitive to the very surface atoms (or more rigorously the surface density of states). For instance, STM was not able to fully decode the structure of the Si(111) 7×7 surface because the majority of the reconstruction was below the topmost layer.

Over the last few years three techniques have risen to prominence for imaging surfaces in a conventional electron microscope; profile imaging where the surface is viewed edge-on [1–3], reflection electron microscopy or imaging RHEED [4,5] and plan-view imaging where the electron beam is normal to the surface of interest [6–8]. Limited initially to a few surfaces with low sticking coefficients such as gold or some oxides, with the advent of UHV microscopes these techniques will play a larger role in the future. What electron microscopy can provide, complementary to other surface science techniques, is information simultaneously about both the surface and the bulk. For profile imaging the basics of interpreting the images using multislice calculations were worked out very early [9] and are essentially the same as those for other high-resolution techniques. Interpretation of reflection electron microscopy imaging is still in its infancy, although there has been substantial progress recently, e.g. refs. [10–12]. For plan-view imaging no systematic study has yet appeared, although there have been a few simulations of surfaces [13], monolayer reconstructions on gold [6,7] and suggestions that diffraction patterns can be interpreted kinematically [14,15].

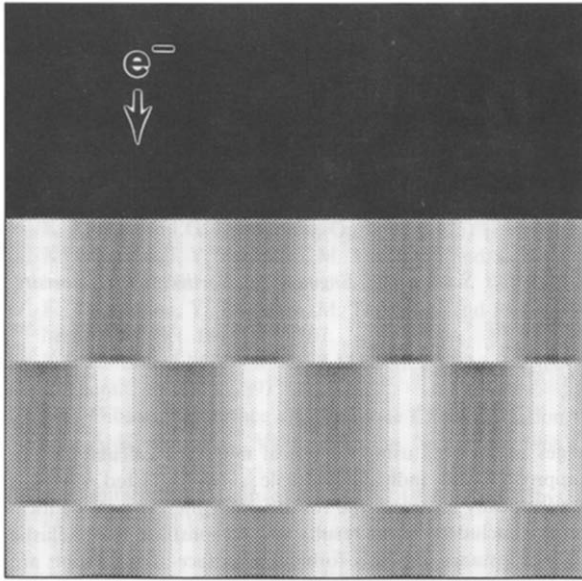


Fig. 1. Grey-scale representation of the potential in a multislice simulation with an abrupt step in between slices, with white corresponding to higher potential regions and the black region at the top represents the vacuum. Note the discontinuities between the slices and at the top surface.

None of these papers have presented a complete or rigorous study, which in many respects is understandable since the technical problems are immense; to simulate a plan-view surface properly one needs very large unit cells and a large number of different slices in the calculations (to simulate the important subsurface distortions) which is impossible with many of the available program packages.

The purpose of this note is to step back a little from direct surface simulations and first test whether the multislice method is valid. It is appropriate to describe why a plan-view simulation might be open to question. A surface leads to a *rel-rod* along the surface normal, and correct representation of this *rel-rod* is central to accurate simulations of a surface. It is often considered that the potential used in multislice is abrupt along the beam direction, e.g. fig. 1, and as such may lead to too much scattering along the beam direction, in *HOLZ* lines for instance [16]. Whereas techniques exist using a three-dimensional sampling [17] to represent the *z*-direction

scattering in a crystal, it is not clear that these are appropriate for a surface where there would be discontinuities in the potential. The presence of discontinuities could be important; in RHEED using a Bloch wave approach it has recently been demonstrated that the method can fail if an inappropriate surface match is used which ignores the potential variations at the surface [18]. If the conventional multislice can be used with standard slices surface simulation becomes relatively trivial; if not, then more work remains. We will focus on simulations relevant to diffraction patterns and dark-field/bright-field imaging since in both the literature and our own results these are more powerful than direct high-resolution imaging which suffers from complications due to strong moiré effects. This also allows inclusion of inelastic scattering by a pragmatic optical potential approach which is of unclear validity for high-resolution imaging.

In the following sections, we will first describe a full three-dimensional method of representing the potential which allows inclusion of the top and bottom surfaces of the crystal as well as better sampling along the beam direction. We then show that this method yields identical results to those obtained from a conventional multislice in both the elastic and inelastic cases focusing on the surface-allowed bulk spots [19] as test "surface sensitive" features. In the process, we verify that these are bulk Bloch-wave states with very small extinction distances which are strongly affected by inelastic scattering. It is also pointed out that there exists a strong top-bottom effect in plan-view surface imaging.

2. Theoretical methods

Conventional numerical calculations were performed using the NUMIS programs on Apollo workstations written at Northwestern by the author; these use the standard multislice approach, details of which can be found in numerous papers, e.g. refs. [20–22]. For reference, it should be mentioned that these programs sum the potential of each atom within any given slice, rather than using a subslice of a projected unit cell. Further-

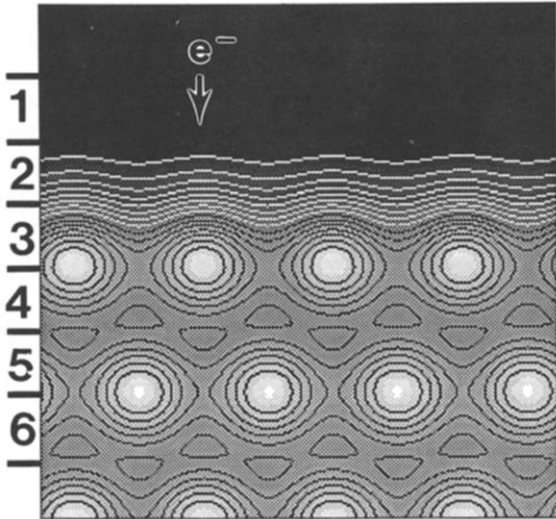
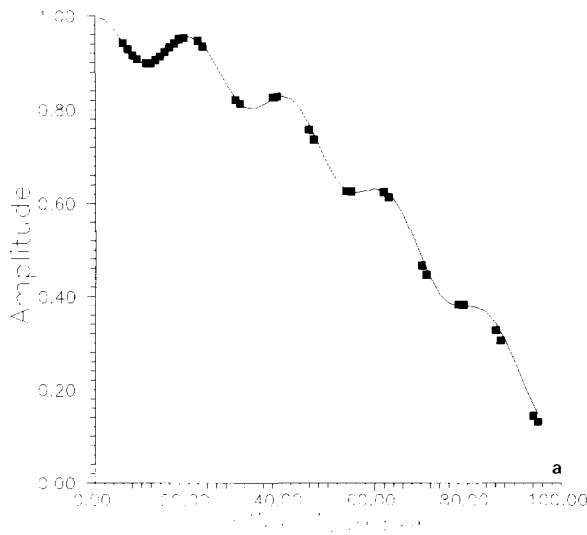


Fig. 2. Illustration of the slice structure for a three-dimensional calculation with a true surface built in, using a grey scale with contour lines superimposed, white regions corresponding to the regions of highest intensity. On the left is shown the regions used for the first 6 slices for a slice thickness of $a_0/4\sqrt{2}$.

more, the calculations were performed with the constraint that (in the absence of inelastic scattering) the total wave intensity remained unity



($\pm 10^{-2}$ or better for a thick crystal). For the more complete simulation including properly the top and bottom surfaces a full three-dimensional potential of samples was evaluated using an analytic continuation to the third dimension of the two-dimensional Gaussian scattering factors. One can write the two-dimensional electron scattering factors for a single atom as:

$$F(u) = \sum a_n \exp(-b_n u^2),$$

with a reciprocal space vector in the x, y plane of u . Analytically continuing along the z direction and invoking spherical symmetry gives

$$F(u) = \sum a_n \exp(-b_n u^2) / 2 \left\{ \operatorname{erf}(\pi[z_{n+1} - z]/\sqrt{b_n}) - \operatorname{erf}(\pi[z_n - z]/\sqrt{b_n}) \right\}$$

for the three-dimensional contribution of an atom at z to the scattering in a slice between z_n and z_{n+1} . With this full potential, calculations were performed as a function of slice thickness. It should be noted that for gold the three-dimensional correction to the potential does not significantly involve atoms more than 6 Å away from

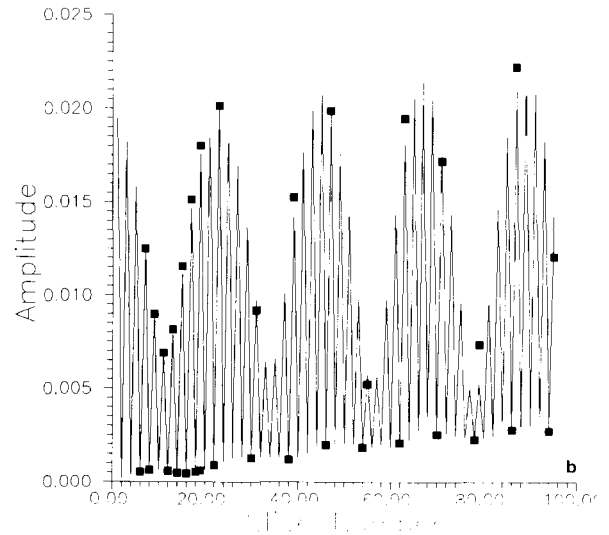


Fig. 3. Graphs of the amplitude of different diffracted beams as a function of slice number ($a_0/2\sqrt{2} = 1.4 \text{ \AA}$ slices) for a gold $1 \times 1 [110]$ surface without inelastic scattering, in (a) for the (000) beam and in (b) for the (110) beam. In both the solid squares are the results for a full crystal with an $a_0/4\sqrt{2}$ slice, and the solid lines are for a conventional multislice with twice this slice thickness.

the slice of interest (along the beam direction). Fig. 2 illustrates the slice structure for the three-dimensional calculations.

Inelastic scattering was included as an imaginary component of the potential, typically 5%; this approach is pragmatic in philosophy, and no attempt was made to explore better models just to determine whether it was a significant issue.

One important issue that should be mentioned concerns numerical accuracy. Some of the calculations were performed using an array processor, and some using a 68030 or 68040 CPU on the Apollo workstations. Although there were only very minor differences between the two for the primary diffracted beams, there were more substantial differences in the forbidden reflections (e.g. {110}, {100}) due to the lower accuracy of the array processor. For instance, the calculations in figs. 3 and 4 used the array processor whereas fig. 6 used the host CPU, and there is a quantitative difference in the thicker regions. Where comparison of methods was relevant, results using the same CPU only were compared; for true quantitative results for thicker crystals full double precision will be required for the weaker diffraction spots.

3. Results

The results of the consistency check are shown in figs. 3 and 4 for a gold [110] zone and, respectively, inelastic and elastic scattering cases using $a_0/2\sqrt{2}$ slices for the conventional multislice and $a_0/4\sqrt{2}$ slices for the three-dimensional case with a 64×64 array. It should be mentioned that the three-dimensional calculations were for complete crystals with top and bottom surfaces included as per fig. 2. Furthermore, the convergences of the three-dimensional calculations were tested using slices of $a_0/2\sqrt{2}$, $a_0/4\sqrt{2}$ and $a_0/8\sqrt{2}$ and they were well converged with the $a_0/4\sqrt{2}$ slices. Within the precision of the single arithmetic calculations, the results are almost identical, certainly far more similar than uncertainties in, for instance, the exact potential and inelastic scattering effect. One feature comparing figs. 3 and 4 is that inelastic scattering is clearly very important. Without it, one predicts that surface steps can be imaged from the forbidden spots at all thicknesses, but with it they can only be detected for very thin crystals. This is consistent with experiments; for very thin evaporated samples they have been readily observed (e.g. ref. [7]), but we

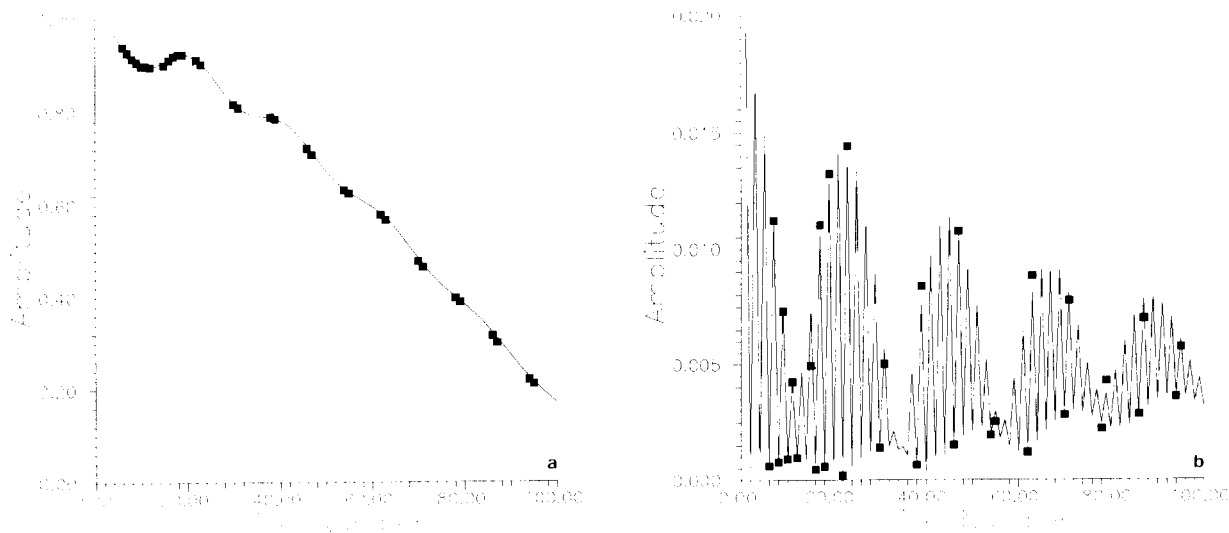


Fig. 4. Graphs of the amplitude of different diffracted beams as a function of slice number ($\sim 0.7 \text{ \AA}$ slices) for a gold 1×1 [110] surface with inelastic scattering of 0.05. The figures correspond to the same conditions as fig. 3.

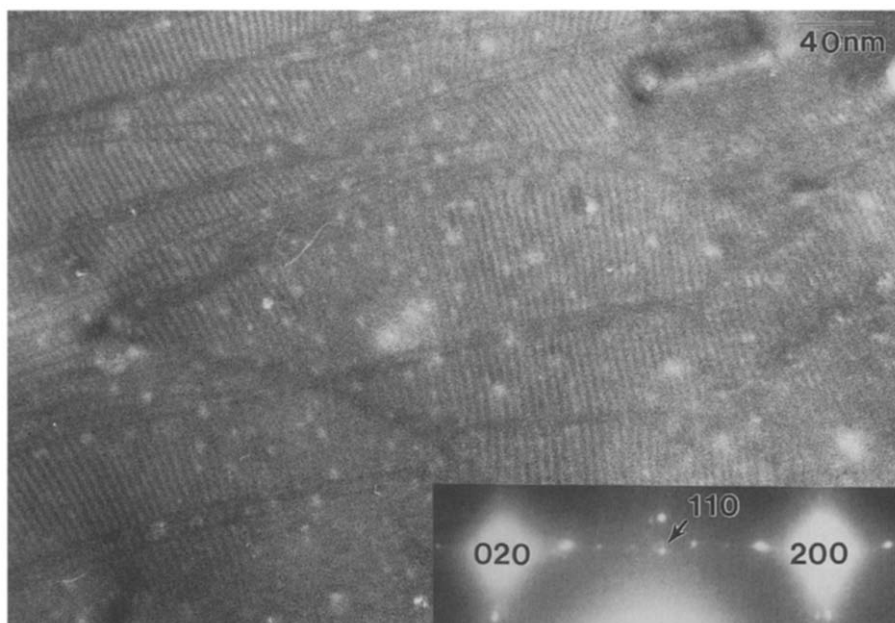


Fig. 5. Experimental image of the gold 5×20 [001] surface, taken from ref. [29] with a sample thickness that is estimated at about 30–40 nm. The wider fringes are the “20” unit of the cell, the finer ones from the “5” unit. The important point is that both top and bottom surfaces should be reconstructed, but the image shows only the features of one surface. This can be attributed to attenuation of the top surface signal by inelastic scattering. Note as well that there is no evidence of any step contrast, although the image was taken with an aperture centered on the forbidden (110) diffraction spot (see inset).

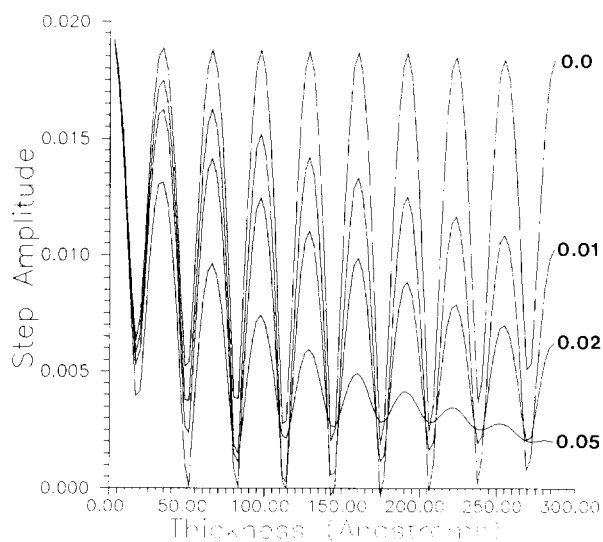


Fig. 6. Graphs of the amplitude of the surface step contrast (difference between the (110) amplitude between adjacent slices) as a function of thickness for various amounts of absorption as indicated on the right.

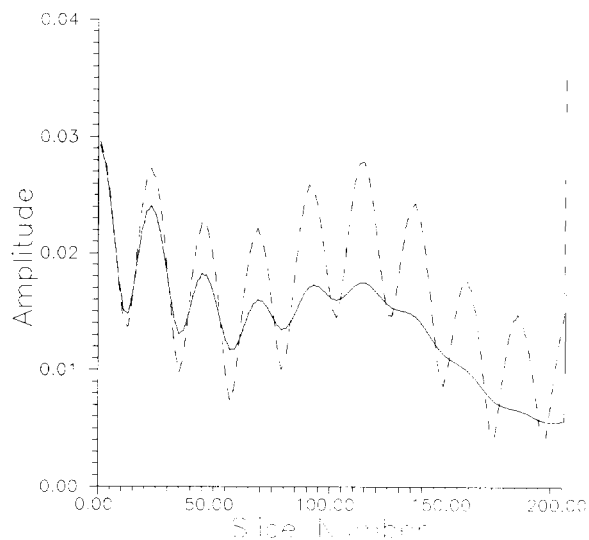


Fig. 7. Graph of the amplitude of the $(6/5, 6/5, 0)$ beam (the primitive diffraction vector of the fcc [111] monolayer on top) as a function of slice number ($a_0/2$ slices) without (dashed) and with (solid) inelastic scattering. Note in both cases the very substantial contribution from the bottom surface.

have not observed them using bulk samples, see for instance fig. 5. The variation of the amplitude of step contrast is shown more clearly in fig. 6 as a function of both thickness and inelastic scattering. The role of inelastic scattering is consistent with the interpretation of the forbidden spots as corresponding to interference between Bloch waves with a very small extinction distance, with preferential absorption of one of the Bloch waves (e.g. ref. [23]). The large excitation error that one would associate with these spots is also consistent with this observation; in simple two-beam model anomalous absorption effects are far more signifi-

cant in damping the thickness oscillations in pseudo-kinematic conditions (e.g. ref. [23]).

An immediate follow-up to this result is that one can expect a strong top-bottom effect in plan-view imaging. As an illustration of this, fig. 7 graphs the intensity of the $(6/5, 6/5, 0)$ reconstruction spot for a gold 5×1 [001] reconstruction [24–26] on the top and on the bottom surface with and without absorption. A 256×64 unit cell was used with $a_0/2$ slices. The bottom surface reconstruction appears to be more readily observable than that on the top surface in both cases. There are two reasons for this. First, the diffrac-

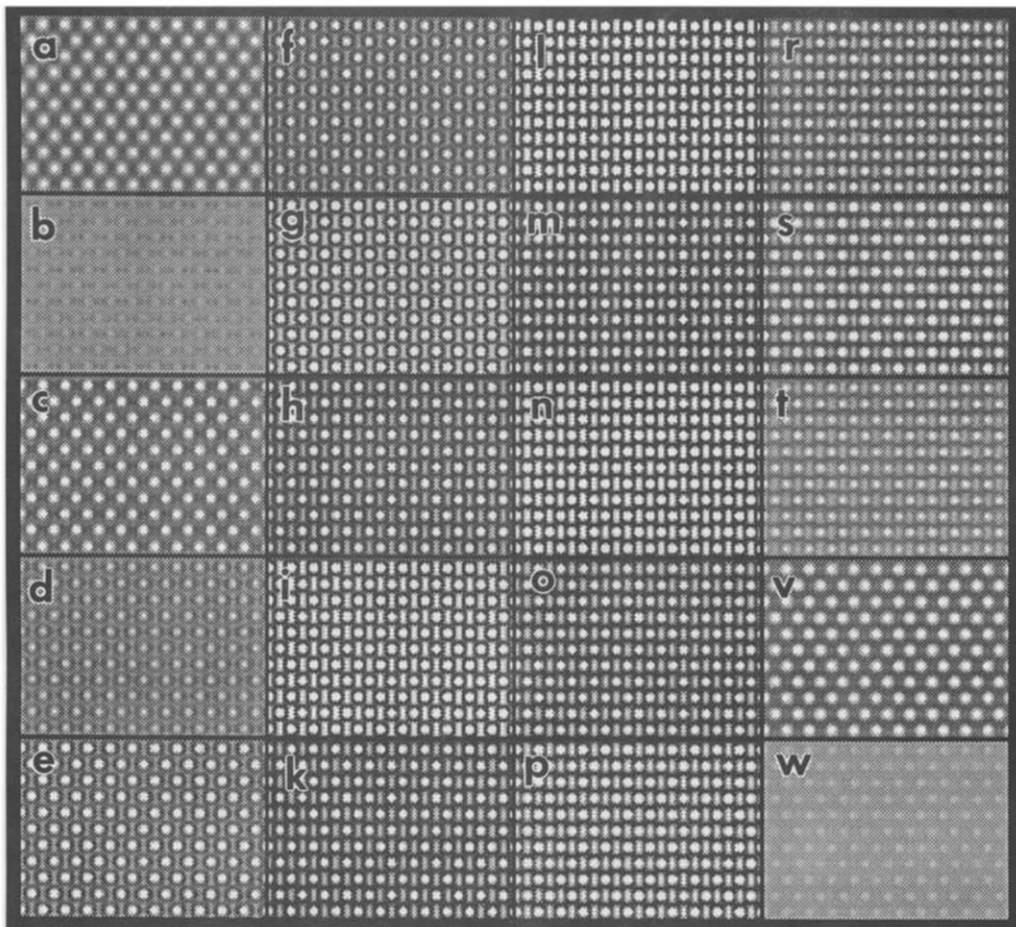


Fig. 8. HREM images on the $[110]$ zone without inelastic scattering with a Cs of 0.9 mm at 300 kV, 0.5 mRad convergence and a focal spread of 8 nm and a defocus of -60 nm with a contrast range from 0.0 to 1.5. From the top left, down and then across in steps of 10 slices (28 \AA). Note the strong second orders in the thicker regions.

tion from the top surface will “diffuse” to higher-angle multiple diffraction spots, and secondly it will be attenuated by the adsorption. Experimental support for this can also be found in fig. 5, where there is only evidence for one domain at each position and no indications of overlapping domains or domain boundaries. However, it should be mentioned that in some cases superposition of domains has been observed which can only be from the top and bottom surfaces, and therefore this conclusion is not as strong as that for the forbidden spots.

4. Discussion

The result that conventional multislice works in the plan-view geometry is useful; as a numerical technique it is far more flexible than a Bloch-wave calculation for a complicated unit cell. However, the sensitivity of the results to inelastic scattering is a little disturbing and will need to be an area for further work. To emphasize this a little more, figs. 8 and 9 show HREM simulations corresponding to the data shown in figs. 3 and 4; there is relatively little effect compared to the

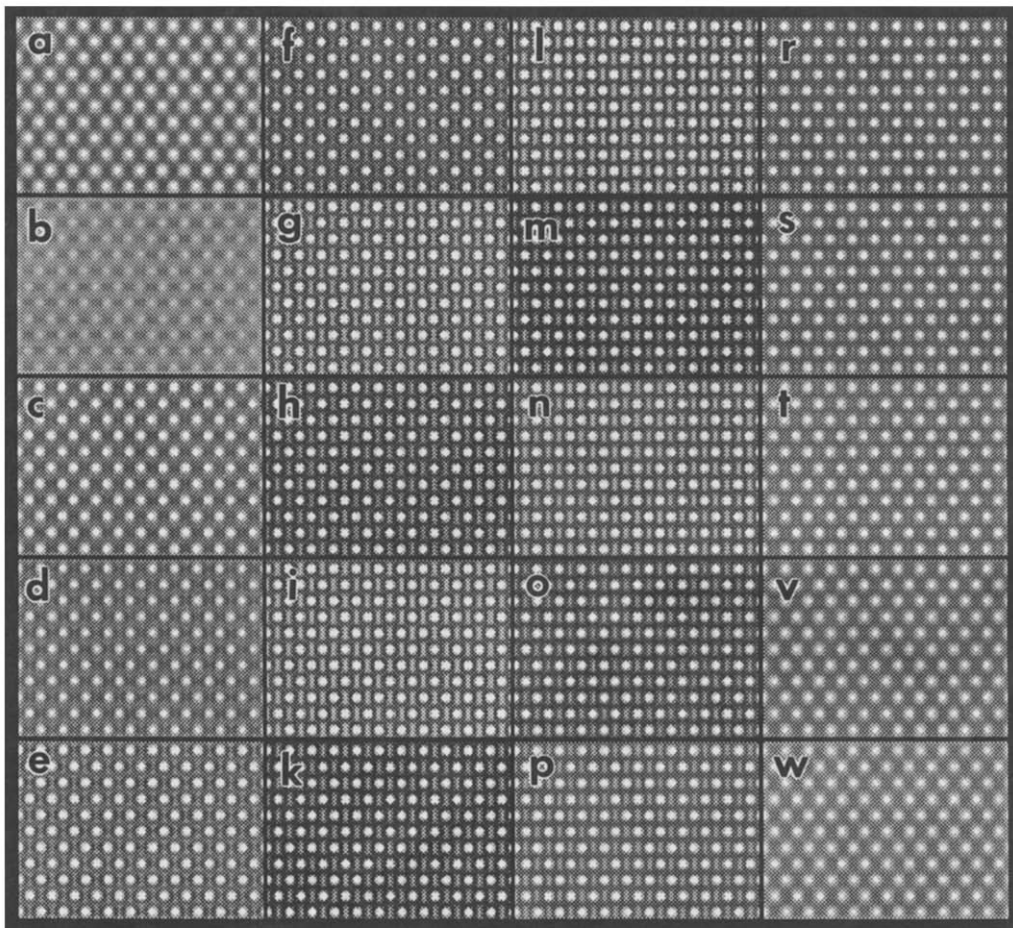


Fig. 9. HREM images on the [110] zone with inelastic scattering of 0.05 and the same conditions as for fig. 8. The mean level has been adjusted up to correspond to the data in fig. 7 without altering the contrast; this assumes that the absorbed component contributes to the diffuse background only. Note that the only major effect is a reduction in the second-order contribution, which is small compared to the effects described above for the forbidden spots.

strong surface effects already demonstrated. For completeness, it should be mentioned that the consistency check has also been applied to the gold 5×1 [001] reconstruction data shown in fig. 6 and for the boron-doped $\text{Si}\sqrt{3} \times \sqrt{3}$ $R30^\circ$ surface for which we have (unpublished) experimental results, and in both cases the conclusions are the same as those described above.

An issue that merits further discussion is why conventional multislice is consistent with three-dimensional calculations, i.e. appears to behave correctly along the beam direction, but tends to produce HOLZ line intensities which are significantly larger than those experimentally observed, e.g. ref. [16]. The answer to this appears to be the inelastic contribution. HOLZ lines are pseudo-kinematical, and as such will be far more strongly affected by absorption than the more dynamical reflections. This conclusion can be seen quite clearly in some recent full simulations of the major inelastic term, i.e. phonon effects, within multislice [27,28]. It appears that multislice, done properly, should be correct, but one must be careful to include inelastic scattering for HOLZ and surface diffraction phenomena.

5. Conclusions

Conventional multislice is consistent with more rigorous calculations and includes the three-dimensional effects important to surface plan-view imaging. Inelastic scattering is of major importance, and cannot be neglected, as evidenced from both experimental and theoretical results.

Acknowledgements

This work was supported by the Air Force Office of Scientific Research on grant number AFOSR 86-0344 DEF. Funding for the UHV microscope was provided by the Keck Foundation, the National Science Foundation and the Air Force Office of Scientific Research, and would have been impossible without the efforts of Robbie Kosak.

References

- [1] L.D. Marks, Phys. Rev. Lett. 51 (1983) 1000.
- [2] L.D. Marks, in: Structure and Dynamics of Surfaces, Eds. W. Schommers and P. von Blackenhagen (Springer, Berlin, 1986).
- [3] D.J. Smith, in: Chemistry and Physics of Solid Surfaces, Eds. R. Vanselow and R. Howe (Springer, Berlin, 1986).
- [4] T. Hsu, S. Iijima and J.M. Cowley, Surf. Sci. 137 (1984) 552.
- [5] N. Shimizu, Y. Tanishiro, K. Takanayagi and K. Yagi, Ultramicroscopy 18 (1985) 453.
- [6] G. Nihoul, K. Abdelmoulas and J.J. Metois, Ultramicroscopy 18 (1985) 435.
- [7] N. Ikarashi, K. Kobayashi, H. Koike, H. Hasekura and K. Yagi, Ultramicroscopy 26 (1988) 195.
- [8] J.M. Gibson, in: Surface and Interface Characterization by Electron Optical Methods, Eds. A. Howie and U. Valdre (Plenum, London, 1988).
- [9] L.D. Marks, Surf. Sci. 139 (1984) 281.
- [10] T.C. Zhao and S.Y. Tong, Ultramicroscopy 26 (1988) 151.
- [11] Y. Ma and L.D. Marks, Acta Cryst. A 46 (1990) 594.
- [12] Z.L. Wang, J. Liu, Ping Lu and J.M. Cowley, Ultramicroscopy 27 (1989) 101.
- [13] K. Takanayagi, Ultramicroscopy 8 (1982) 287.
- [14] J.C.H. Spence, Ultramicroscopy 11 (1983) 117.
- [15] Y. Tanishiro and K. Takanayagi, Ultramicroscopy 27 (1989) 1.
- [16] L.C. Qin and K. Urban, Ultramicroscopy 33 (1990) 159.
- [17] R. Kilas, M.A. O'Keefe and K.M. Krishnan, Ultramicroscopy 21 (1987) 41.
- [18] Y. Ma and L.D. Marks, Acta Cryst., in press.
- [19] D. Cherns, Phil. Mag. 36 (1977) 1429.
- [20] J.M. Cowley and A.F. Moodie, Acta Cryst. 10 (1967) 609.
- [21] P. Goodman and A.F. Moodie, Acta Cryst. A 30 (1974) 280.
- [22] P.G. Self, M.A. O'Keefe, P.R. Busek and A.E.C. Spargo, Ultramicroscopy 11 (1983) 35.
- [23] P. Hirsch, A. Howie, R.B. Nicholson, D.W. Pashley and M.J. Whelan, Electron Microscopy of Thin Crystals (Krieger, New York, 1977).
- [24] J. Perdereau, J.P. Biberian and G.E. Rhead, J. Phys. F 4 (1974) 798.
- [25] J.F. Wendelken and D.M. Zehner, Surf. Sci. 71 (1979) 178.
- [26] M.A. Van Hove, R.J. Koestner, P.C. Stair, J.P. Biberian, L.L. Kesmodel, I. Bartos and G.A. Somorjai, Surf. Sci. 103 (1981) 189.
- [27] R.F. Loane, P. Xu and J. Silcox, Acta Cryst. A 47 (1991) 267.
- [28] P. Xu, R.F. Loane and J. Silcox, Acta Cryst., submitted.
- [29] D. Dunn, J.P. Zhang and L.D. Marks, Surf. Sci. 260 (1992) in press.